

1
2 **The architecture of submarine monogenetic volcanoes – insights from 3D**
3 **seismic data**

4
5 P. Reynolds^{1*}, N. Schofield², R.J. Brown³, S. Holford¹
6

7 ¹ Centre for Tectonics, Resources and Exploration (TRaX), Australian School of Petroleum,
8 University of Adelaide, Adelaide, SA 5005, Australia

9 ² Department of Geology & Petroleum Geology, University of Aberdeen, Aberdeen AB24 3UE, UK

10 ³ Department of Earth Sciences, Durham University, Science Labs, Durham, DH1 3LE, UK

11 *Corresponding author: peter.reynolds@adelaide.edu.au, +61484607355
12

13 **Abstract**

14 Many prospective sedimentary basins contain a variety of extrusive volcanic products that are
15 ultimately sourced from volcanoes. However, seismic reflection-based studies of magmatic rift basins
16 have tended to focus on the underlying magma plumbing system, meaning that the seismic
17 characteristics of volcanoes are not well understood. Additionally, volcanoes have similar
18 morphologies to hydrothermal vents, which are also linked to underlying magmatic intrusions. In
19 this study, we use high resolution 3D seismic and well data from the Bass Basin, offshore southern
20 Australia, to document 34 cone- and crater-type vents of Miocene age. The vents overlie magmatic
21 intrusions and have seismic properties indicative of a volcanic origin: their moderate–high amplitude
22 upper reflections and zones of “wash-out” and velocity pull-up beneath. The internal reflections of
23 the vents are similar to those found in lava deltas, suggesting they are composed of volcanoclastic
24 material. This interpretation is corroborated by data from exploration wells which penetrated the

25 flanks of several vents. We infer that the vents we describe are composed of hyaloclastite and
26 pyroclasts produced during submarine volcanic eruptions. The morphology of the vents is typical of
27 monogenetic volcanoes, consistent with the onshore record of volcanism on the southern Australian
28 margin. Based on temporal, spatial and volumetric relationships, we propose that submarine
29 volcanoes can evolve from maars to tuff cones as a result of varying magma-water interaction
30 efficiency. The morphologies of the volcanoes and their links to the underlying feeder systems are
31 superficially similar to hydrothermal vents. This highlights the need for careful seismic interpretation
32 and characterization of vent structures linked to magmatic intrusions within sedimentary basins.

33

34 **I. Introduction**

35 Many magmatic rift basins are characterised by mafic volcanism, which produces a combination
36 of both extrusive and intrusive components. Extrusive components include vent-like features that
37 are volcanic (e.g. Bell & Butcher, 2002; Davies *et al.*, 2005; Thomson, 2007; Wall *et al.*, 2010; Calvès
38 *et al.*, 2011; Jackson, 2012; Magee *et al.*, 2013b; Zhao *et al.*, 2014; Schofield *et al.*, 2015) or
39 hydrothermal in origin (e.g. Jamtveit *et al.*, 2004; Svensen *et al.*, 2004; Planke *et al.* 2005; Hansen,
40 2006; Grove, 2013; Magee *et al.*, 2013a; Magee *et al.*, 2013b; Magee *et al.*, 2015; Alvarenga *et al.*,
41 2016). However, the criteria for distinguishing these vents in seismic data were until now lacking.

42 Volcanoes are composed of either fragmental or coherent volcanic rock. They link the extrusive
43 and intrusive components of volcanic provinces and in-part determine their architecture (e.g.
44 Valentine & Cortés 2013; Re *et al.*, 2015). Their eruption mechanisms vary from magmatic volatile-
45 dominated (eruptions resulting from the expansion of magmatic volatiles) to phreatic (heating of
46 ground or surface water by magma) and phreatomagmatic (resulting from the physical mixing of
47 ground or surface water with magma) (Sigurdsson *et al.*, 2015). Volcanoes can be used to identify
48 structural trends, stratigraphic relationships and feeder systems that can be difficult to image in

49 seismic data; thus providing insights into the subsurface geology (e.g. Ebinger *et al.*, 1989; Connor &
50 Conway, 2000; Schofield *et al.*, 2015). They also have the potential to act as hydrocarbon reservoirs,
51 since the volcanoclastic rocks of which many volcanoes are composed can have high permeabilities
52 and porosities (e.g. Magara, 2003; Schutter 2003; Holford *et al.*, 2012).

53 Hydrothermal vents have eye, dome or crater-like shaped upper parts (Planke *et al.* 2005; Grove,
54 2013) underlain by a sandstone dyke or breccia pipe that connects at depth to the tips of a sill
55 (Jamtveit *et al.*, 2004). Based on observations from seismic data, these connection zones have
56 confusingly been referred to as diatremes (Hansen, 2006) a feature diagnostic of volcanoes (White
57 & Ross, 2011). Hydrothermal vents may act as fluid migration pathways long after their burial
58 (Svensen *et al.*, 2003). Moreover, their upper parts may represent a hydrocarbon play (Grove, 2013).
59 The vents have been interpreted to arise from either phreatic or phreatomagmatic activity (Jamtveit
60 *et al.*, 2004) yet there are no descriptions of the juvenile clasts indicative of a phreatomagmatic
61 origin.

62 Well data indicates hydrothermal vents are dominantly composed of remobilised sediment
63 sourced from above the sill, which is subsequently effused from a central vent during a series of
64 pulses (Grove, 2013). The upper parts of hydrothermal vents from the North Atlantic are composed
65 of disaggregated gravel to silt-sized clasts of quartz, woody fragments, pelagic sediments and minor
66 carbonaceous debris (Grove, 2013). Well data from other vent complexes indicates they are
67 composed of diatomitic siltstone with carbonate layers (Svensen *et al.*, 2003) and sandstone,
68 sediment breccia and claystone (Svensen *et al.*, 2006). Some vents also contain clasts of dolerite
69 thought to be sourced from an intrusion (Grove, 2013) although the genesis (e.g. magma-sediment
70 interaction or hydroclastic fragmentation) and source of the clasts (e.g. the allied or a superjacent
71 intrusion) is not described. Volumetrically minor components of volcanic clasts have also been
72 documented from boreholes drilled through the breccia pipes in the Karoo (Svensen *et al.*, 2007).

73 The main concentrations of these clasts occur close to the sill (Svensen *et al.*, 2007); whether these
74 “mixtures” of volcanic and sedimentary material result from magma-sediment interaction or
75 otherwise is unclear.

76 Given the similar morphologies of hydrothermal vents and volcanoes, their similar location
77 within volcanic provinces, and their relationship to underlying sills, it has proved difficult to
78 distinguish between them. For instance, based on observations of the feeder system, early workers
79 proposed that some hydrothermal vents within the Karoo are almost wholly composed of volcanic
80 material (Jamtveit *et al.*, 2004 and references there-in). However, later work revealed that these
81 features represent feeders for volcanoes formed during phreatomagmatic activity (McClintock *et al.*,
82 2008). In seismic data, the origin of some vents has only been confirmed following drilling (Davies
83 *et al.*, 2002; Grove, 2013). Further hampering the identification of volcanoes is the fact that
84 monogenetic volcanoes display a variety of morphologies, some of which are unresolvable due to
85 their height and basal diameter being below the vertical resolution and line spacing of 2D seismic
86 surveys.

87 This study uses 3D seismic and well data to describe the facies architecture of Miocene-aged
88 submarine volcanoes formed offshore southern Australia. These volcanoes are found at shallow
89 depths (1208 metres below sea floor) and are free from overlying basalt cover, making them ideal
90 candidates for study. We provide a detailed assessment of their architecture, allowing us to highlight
91 the criteria for distinguishing between types of vents in seismic data. We also provide insights into
92 how their morphologies varied as a result of varying magma-water mixing.

93

94 **2. Geological setting and Dataset**

95 The southern margin of Australia formed as a result of Gondwanan rifting that commenced in
96 the Middle–Late Jurassic, culminating in breakup in the Campanian (Totterdell & Bradshaw, 2004).

97 The margin is characterised by a series of east-west trending rift basins and an abundance of both
98 offshore and onshore intraplate igneous rocks (e.g. Holford *et al.*, 2012; Ball *et al.*, 2013). Magmatism
99 has been linked to late-stage rifting processes at a craton margin (Ball *et al.*, 2013), impingement of
100 a mantle plume (Davies *et al.*, 2015) or shear- and edge-driven mantle convection (Meeuws *et al.*,
101 2016). Many of the volcanoes are monogenetic in origin, and range from Jurassic to Recent in age
102 (Johnson, 1989; Cas *et al.*, 1993). Onshore volcanism in the Newer Volcanic Province, southern
103 Australia, is characterised by maars, scoria cones, tuff cones and lava flows, produced during
104 subaerial and submarine volcanic activity (Cas *et al.*, 1993). Despite the abundance of volcanism, the
105 margin is classified as magma-poor due to the late stage arrival of relatively low volumes of magma
106 (Norvick & Smith, 2001; Sayers *et al.*, 2001; Holford *et al.*, 2012; Ball *et al.*, 2013).

107 The Bass Basin is located offshore between Victoria and northern Tasmania (Fig. 1). It represents
108 a failed intra-cratonic rift basin (Blevin, 2003) and consists of a series of Cretaceous northwest-
109 southeast trending half-grabens (Holford *et al.*, 2012). As summarised by Blevin (2003), the basin fill
110 is characterised by a transgressional sequence, developing from a terrestrial sequence in the Mid
111 Eocene to shallow marine in the present day. Fluvio-lacustrine sequences are found in the Late
112 Cretaceous to Mid Eocene, characterised by the Eastern View Coal Measures (EVCM). Marine
113 transgression continued from the Middle Eocene onwards, forming an estuarine and shallow marine
114 embayment. The overlying Oligocene and Miocene Torquay Group is composed of shallow marine
115 marl and limestone, deposited during continued sea level rise.

116 The Bass Basin also contains a variety of Cretaceous–Miocene-aged igneous features, many of
117 which have been penetrated by petroleum exploration wells (Holford *et al.*, 2012; Table 1). The
118 oldest are Cretaceous volcanoclastic sandstones, although the source of these is unclear (Holford *et*
119 *al.*, 2012). Subsequent Mid-Cretaceous volcanism produced a series of volcanoes, flows and sills
120 (Blevin, 2003; Trigg *et al.*, 2003; Holford *et al.*, 2012). Volcanism peaked in the Palaeocene and

121 Oligocene-Miocene, evidenced by widespread lavas, sills and dykes found through the central and
122 north-east Bass Basin (Blevin, 2003).

123 This study utilises 3D seismic data from the Yolla and Labatt marine surveys which were
124 acquired in 1994 and 2008 respectively. These surveys were acquired with streamer lengths of 3 km
125 and 6 km. We use the PreStack Time Migrated data displayed with SEG Normal polarity. The 525
126 km² Labatt survey has a bin size of 25 × 12.5 m. The Yolla survey is smaller, covering 260 km² with
127 a 25 × 12.5 m bin size. A 2D seismic line is used to tie these two surveys (section A–A', Figs. 1 and
128 2) and also intersects the Bass-I well which penetrates the flanks of a vent.

129

130 **3. Methodology**

131 The vents occur at three separate levels within the Miocene succession of the Bass Basin (Fig.
132 2). We therefore mapped three pairs of Base and Top Volcanic surfaces which bound the vents,
133 which are numbered according to their stratigraphic position. The vents in the Yolla survey are
134 oldest and occur towards the base of the Miocene Torquay Group; these are the TV1 and BV1
135 horizons which have been tied using a synthetic seismogram from the Yolla-I well. This well
136 penetrated 68 m of volcanic rocks between 1237 and 1305 m (Fig. 3). The vents in the Labatt
137 survey, which are not penetrated by wells, have been mapped using the TV2 and BV2 horizons (Fig.
138 2). The youngest vents occur within sediments of mid-late Miocene age, and have been mapped using
139 the TV3 and BV3 horizons. These horizons are tied to the Bass-I well, which penetrated 160 m of
140 volcanic rocks between 790 and 950 m (Fig. 3). Horizons TV1, TV2 and TV3 are peak events that
141 define the onlap surface of the vents and vary from moderate to high amplitude. The dominant
142 frequency at the TV2 horizon is 45 Hz and the dominate frequency of the TV1 is 39 Hz, indicating
143 the vertical resolution is 15–20 m in the Labatt and Yolla surveys respectively. The BV1–BV3
144 horizons are trough events that define the horizon downlapped by the vents' internal reflections,

145 and vary from high to low amplitude. The horizons are mapped locally beneath the vents and are
146 often poorly imaged beneath their central parts. Detailed mapping of the TV2, BV2 and TV1 and
147 BVI horizons allowed us to investigate the distribution and morphology of the vents in the Labatt
148 (Figs. 4 and 5) and Yolla surveys respectively (Figs. 4 and 6).

149 Many of the vents are underlain by seismic velocity pull-ups (Fig. 2). The height of the velocity
150 pull-up relative to the regional base datum was used to calculate the internal velocity of each vent,
151 using the method defined by Magee *et al.* (2013b). This gave each vent a value of between 2200 and
152 4025 m s⁻¹ (assuming a velocity of 2090 m s⁻¹ for the Miocene Torquay Group; as constrained from
153 Yolla-I well data). Where pull-ups were absent beneath a vent, a velocity of 2090 m s⁻¹ was used.
154 These velocities were used to calculate the vent heights and are accurate to within 100 m (allowing
155 for a velocity variation of 600 m s⁻¹ within the Miocene Torquay Group).

156 The Labatt survey contains several sills (Fig. 4). These are recognised by high amplitude,
157 continuous reflections that cross cut adjacent reflections (e.g. Thomson & Hutton, 2004; Holford *et al.*,
158 2012). The dominant frequency at the depths at which the sills are found is ~40 Hz in both
159 surveys, suggesting the sills need to be >30 m thick to be resolved and >13 m thick to be detected.
160 We use a velocity of 3000 m s⁻¹ (as constrained from the Bass-I well; see Trigg *et al.*, 2003) to
161 calculate the depth of the sills beneath the BV2 horizon.

162

163 **4. Vent characteristics**

164 **4.1 Vent morphology**

165 The vents can be categorised into cone- and crater-types according to their morphology (Fig. 7;
166 Table 2). The crater-types (Fig. 7A) are represented by sub-circular excavations in the TV2 surface
167 which range from 340–1200 m in diameter, and are underlain by <300 m wide, funnel-shaped
168 features that extend 50–100 m into the subsurface. The crater-type vents are only found in the

169 Labatt survey. Their craters are filled with low amplitude, sub-horizontal reflections which onlap the
170 crater margins and are surrounded by concentric faults. The cone-type vents, which are found in
171 both surveys, include: 1) pointed; 2) cratered, and 3) flat topped morphologies. These vents have
172 sub-circular bases, are roughly symmetrical in plan view and have a distinctive onion-ring structure
173 in time slice. Their flanks dip 5–18° and their basal diameter and height increases as their volume
174 increases (Fig. 7E and F). The pointed vents have a conical morphology (Fig. 7B). They overlie the
175 crater-type vents. The cratered vents (Fig. 7C) are characterised by an upper bowl-shaped reflection
176 that defines a ~30 m deep crater in the centre of the edifice. The flat-topped vents (Fig. 7D) lack
177 craters and instead have sub-horizontal tops.

178

179 **4.2 Seismic facies**

180 Internally, the cone-shaped vents are composed of two differing seismic facies which are
181 distinguished on the basis of the reflection amplitude, morphology and facies geometry. Seismic
182 facies 1 (SF1) is composed of moderate to high amplitude reflections with a hummocky character
183 (Fig. 7B–D). They only occur within the vent flanks. The reflections vary from semi-continuous to
184 continuous and form wedge-shaped packages ≤ 0.2 s thick. They are oriented sub-parallel to the TV1
185 and TV2 horizons. The facies downlaps the BVI and BV2 horizons and progrades laterally from the
186 centre of the vent which is commonly composed of seismic facies 2 (SF2). This facies is composed
187 of low amplitude, discontinuous reflections that grade laterally into SF1. SF2 forms plug-like bodies
188 up to 2 km wide in the central part of the vents (Fig. 7B–D). This facies is oriented oblique to the
189 TV1 and TV2 horizons and may truncate the BVI and BV2 horizons, extending beneath the vents
190 for ≤ 0.2 s.

191 The reflections overlying the vents are sub-parallel in orientation and have low amplitudes.
192 Polygonal faulting is observed in a ~ 0.1 s-thick sequence of reflections overlying the vents at ~ 0.6 s

193 and ~0.8 s in the Labatt and Yolla surveys respectively. The reflections are commonly domed above
194 the vents (Figs. 2, 5 and 6) and are disrupted by vertical pipe-like features above the summit of the
195 vent drilled by the Yolla-I well (Fig. 6).

196

197 **4.3 Spatial Distribution**

198 Within both the Labatt and Yolla surveys, the vents form linear rows, or occur as isolated vents
199 (Figs. 5 and 6). Those in rows are spaced 800–3000 m apart and contain up to four individual vents,
200 which onlap in a northerly direction and decrease in volume towards the south. The rows are
201 oriented approximately north-south, and overlie north-south oriented grabens. 23% of the isolated
202 vents do not overly faults, while the remaining 77% are found above the upper tips of normal faults.

203 Sills are only found beneath the isolated vents within the Labatt survey. They occur 500–1200
204 m beneath 8% of the vents. These sills have a saucer- or layer-parallel shape and range from 2–4 km
205 in diameter. They occur as isolated bodies and do not form vertically interconnected complexes
206 with adjacent sills. The sills have tips which shallow beneath the centres of the vents (Fig. 8). The
207 sills are connected to the overlying vents by a zone of velocity pull-up roughly equal in width to that
208 of the vent. No evidence of forced folding is observed above the sills. The remaining 92% of the
209 vents are not visibly connected to an underlying sill and are underlain by regions of poor imaging
210 and velocity pull-up.

211

212 **5. Interpretation**

213 **5.1 Environment of formation**

214 The vents are interpreted to have formed in a shallow marine environments, evidenced by the
215 transgressional sequence within which the vents are found and the overlying marls and limestones
216 (e.g. Boreen & James, 1995). An extrusive origin for the cone-shaped vents is indicated by the

217 reflections which onlap the vents, and the reflections within the vents which downlap the underlying
218 horizon. The doming of reflections above the vents is typical of differential compaction, suggesting
219 that the vents are composed of denser rock than the overlying sediments. The fact that the vents
220 are found at different stratigraphic levels (Fig. 2) clearly indicates that vent formation was not
221 synchronous across the Bass Basin.

222

223 **5.2 Preservation of the vents**

224 The cone-type vents are not interpreted to be the erosional “stumps” of larger edifices, since
225 the vents retain no evidence for erosion such as wave-cut platforms or erosional rills and gullies.
226 Furthermore, they preserve features such as craters (e.g. Fig. 7C) that suggest they are preserved
227 in a near-pristine state. Other vents along the southern Australian margin constructed in a submarine
228 environment are similarly preserved in a near-pristine state; Jackson (2012) attributes this to 1)
229 rapid flooding of the vents during eustatic sea level rise; 2) the location of the vents on the outer
230 shelf, reducing wave and tidal erosion; 3) weak post-Eocene ocean currents, and 4) no caldera
231 collapse. We infer similar processes for the vents in this study, and highlight also that caldera collapse
232 is only typical of large polygenetic volcanoes, unlike the vents in this study (see following section).

233

234 **5.3 Evidence for a volcanic origin**

235 Numerous exploration wells within the Bass Basin have penetrated intrusive and extrusive
236 volcanic rocks identified in wireline logs, cuttings and sidewall cores (Table 1). For example, the
237 Bass-I well was drilled to test the hydrocarbon potential of a Miocene “reef complex”. This reef
238 complex was subsequently shown to be a volcano, as the well intersected a 160 m-thick sequence
239 of volcanic rocks interpreted as pyroclastic deposits (Blevin, 2003; Trigg *et al.*, 2003). The Yolla-I

240 well also intersected a 68 m-thick sequence of fragmental volcanic rock, interpreted to represent
241 highly altered pyroclastic deposits (Blevin, 2003). This indicates that the vents are volcanic in origin.

242 The seismic characteristics of the vents are also typical of volcanic lithologies; the TV1 and TV2
243 horizons are high amplitude relative to the overlying reflections (Figs. 5 and 6). This indicates that
244 the TV1 and TV2 surfaces represent a high acoustic impedance boundary. The cone-shaped vents
245 also produce pull-up features beneath them; typical of volcanic rocks within a sedimentary sequence
246 (Jackson, 2012; Magee *et al.*, 2013b). The calculated velocities of the vents (section 3) is higher than
247 that reported for hydrothermal vents ($<1800 \text{ m s}^{-1}$; see Svensen *et al.*, 2003) yet lower than that of
248 lava flows (commonly $3300\text{--}6800 \text{ m s}^{-1}$; see Planke & Eldholm, 1994; Nelson *et al.*, 2009). This
249 suggests that the cone-shaped vents are dominantly composed of fragmental, volcanoclastic material
250 (e.g. pyroclasts and hyaloclastite) as opposed to lavas that typify effusive, subaerial volcanic eruptions,
251 or sands and silts that typify hydrothermal vents (e.g. Grove 2013).

252 Volcanoclastic deposits such as pyroclasts and hyaloclastite are typical products of submarine
253 eruptions (e.g. Kokelaar, 1986; Suiting & Schmincke, 2009; Watton *et al.*, 2013a), consistent with the
254 interpreted emplacement environment of the vents. Hyaloclastite has variable grain sizes and
255 vesicularities (e.g. Watton *et al.*, 2013a; Watton *et al.*, 2013b). These properties affect the velocity
256 and hence seismic amplitude of the component facies, and could produce a seismic reflection of
257 moderate or high amplitude, such as that which typifies the TV1 and TV2 horizons. Facies similar to
258 SF1 which typify the flanks of the vents are reported in other seismic datasets from volcanic margins,
259 and represent hyaloclastite at the fronts of lava deltas (e.g. Planke *et al.*, 2000; Wright *et al.*, 2012).
260 Poor imaging in regions represented by SF2 may result from the high impedance contrast of the TV1
261 and TV2 horizons. Furthermore, this central region may contain numerous dykes intruded into the
262 edifice, creating high velocity contrast between fragmental and coherent volcanic material.

263 Our interpretation that the vents are volcanic in origin is consistent with the long-lived, episodic
264 record of magmatism onshore. The southern margin of Australia has experienced volcanic activity
265 since the Jurassic to the near present day, much of which is monogenetic in origin. Miocene examples
266 of pillow lavas and submarine basalts outcrop on the northern coast of Tasmania (Fox et al., 2016)
267 whilst the most recent expression of volcanism along the margin is found in the Newer Volcanic
268 Province (aged 4.5 Ma to 4.5 kyr) in Victoria. This province is typified by over 400 tuff cones, lava
269 flow, maars and scoria cones (Boyce et al., 2014). Here and elsewhere along the onshore southern
270 Australian margin, no hydrothermal vents are recognised.

271 The vents in our study also share many morphological characteristics with volcanoes. The
272 volumes of the cone and crater-type vents are typical of monogenetic volcanoes (commonly $<1 \text{ km}^3$;
273 see White & Ross, 2011). The distance at which the vents are spaced in linear rows is also typical
274 of volcanoes aligned along fissures (Thordarson & Self, 1993). The pit craters have similar dimensions
275 to maars; these are explosion craters in the country rock with diameters of 0.2–3 km (White &
276 Ross, 2011). The funnel-shaped conduits beneath the pit craters have similar dimensions and
277 morphologies to diatremes, which underlie maars (White & Ross, 2011). The ejecta rings that
278 surround maars are commonly $<30 \text{ m}$ in height and are not recognised, perhaps due to altered
279 depositional regimes in the submarine environment. The pointed vents are interpreted to be pillow
280 volcanoes (Batiza & White, 2000) a type of submarine volcano that forms during the subaqueous
281 effusion of basaltic lava. Pillow volcanoes are of similar dimensions to the pointed edifices and
282 similarly lack a crater (Batiza, & White, 2000). They are composed of volcanoclastic material
283 (hyaloclastite and pillow lavas). Pillow volcanoes represent the early stages of tuff cone growth (e.g.
284 Moore, 1985). The cratered and flat-topped edifices are interpreted as monogenetic tuff cones on
285 the basis of their similar size and similar crater dimensions (White & Ross, 2011). Tuff cone-forming

286 eruptions may effuse lava in the later stages (Moore, 1985) and the flat topped vents are interpreted
287 as tuff cones within which lavas and/or hyaloclastite has filled their crater.

288 The facies and architecture of the vents identified in this study are broadly similar to those of
289 the submarine volcanoes and shield volcanoes described by Bell & Butcher (2002) and Magee *et al.*
290 (2013b). These volcanoes have onion ring structures in plan view, high amplitude tops and
291 prograding reflections in their flanks. Zhao *et al.* (2014) describe “volcanic mounds” from the South
292 China Sea, which have a similar size and depth relationship to sills to the vents we describe.
293 However, these features lack detailed description to provide further comparison. The pit craters
294 have a similar size, and morphology to the maars described by Wall *et al.* (2010), in which dykes are
295 clearly imaged beneath the maar using magnetic data.

296 The spatial relationship between the sills and vents suggests that the sills acted as feeders for the
297 vents (Fig. 8). Furthermore, the intrusion penetrated by the Cormorant-I well (Table 1) was of
298 Miocene age (Sutherland & Wellman, 1986) suggesting that the vents and sills are temporally related.
299 Our hypothesis is supported by other datasets which also indicate that sills can act as feeders for
300 eruptions (Muirhead *et al.*, 2016). The vents that lack underlying sills are interpreted to have been
301 fed by dykes, which are difficult to image in seismic datasets due to their sub-vertical orientation and
302 narrow width (<several metres). Beneath the crater-type vents, these dykes are inferred to have
303 transitioned into diatremes in the shallowest subsurface (i.e. less than a hundred metres). Similar
304 feeder relationships are inferred beneath other submarine volcanoes (e.g. Suiting & Schmincke,
305 2012). Since there are few sills within the dataset, we infer that dykes formed the dominant
306 mechanism of magma transport to the paleosurface. Our data supports other studies which infer
307 that dykes play the dominant role in transporting magma to the surface in monogenetic volcanic
308 fields, both along parts of the southern Australian margin (e.g. Holt *et al.*, 2013) and in other
309 monogenetic volcanic fields (e.g. Muirhead *et al.*, 2016).

310

311 **6 Discussion**

312 **6.1 Temporal evolution of the vents**

313 We infer that the mapped Bass Basin vents represent ancient volcanoes “frozen” at different
314 stages of their development, allowing for the evolution of the volcanoes to be established from an
315 early of stage formation through to late stage full vent construction (Fig. 7). This interpretation is
316 supported by superposition relationships and volume trends. The pit craters are directly overlain by
317 pointed vents, indicating that the pit craters formed first. The cratered and flat-topped types are
318 generally of larger volume than the pointed vents. We infer that the cratered and flat-topped vents
319 represent older vents preserved in later stages of their evolution. The volcanoes may thus begin as
320 maar-diatreme complexes on the seafloor (represented by the crater-type vents) in which magma
321 fragmentation occurred beneath the subsurface (Fig. 9A). Continued magma supply is inferred to
322 have led to the construction of the pillow volcanoes (represented by the pointed vents; see Fig. 9B).
323 Growth of the volcanoes towards the sea surface resulted in the formation of tuff cones
324 (represented by the cratered vents; Fig. 9C). The late-stage ponding of lavas and/or hyaloclastite
325 within the tuff cone craters formed the flat-topped volcanoes.

326

327 **6.2 Potential for the misidentification of volcanoes as hydrothermal vents**

328 Volcanic-affected basins contain a range of vents which can be hydrothermal or volcanic in origin
329 (e.g. Fig. 10; Table 3). Both types of vents form mound-shaped features on the pre-eruptive surface
330 (Fig. 10), have similar volumes and dimensions (e.g. Planke *et al.*, 2005) and occur in linear rows (e.g.
331 Grove, 2013). Additionally, both volcanoes and hydrothermal vents may be underlain by narrow
332 chimney zones (Fig. 10) that connect to underlying sills at 0.7–3 km depth. Despite these similarities,

333 our study has shown that well data and detailed seismic mapping can be used to distinguish between
334 these types of vents.

335 The Bass-I and Yolla-I wells indicate that the volcanoes within the Bass Basin are composed of
336 volcanoclastic material with seismic velocities of 2090–4025 m s⁻¹. In comparison, hydrothermal vents
337 along the Northeast Atlantic margin have seismic velocities of 1800 m s⁻¹ and their upper parts are
338 composed of diatomitic siltstone, carbonate and sandstone (Svensen *et al.*, 2003; Grove, 2013). In
339 basins which lack wells penetrating the upper parts of vents, we suggest seismic facies analysis can
340 be used to distinguish between volcanoes and hydrothermal vents. The volcanoes we describe have
341 moderate-high amplitude upper reflections (the TV1 and TV2 horizons) unlike the Top Vent
342 reflections of hydrothermal vents which are low-moderate amplitude (Fig. 10). Internally, the
343 volcanoes we describe have moderate-high amplitude hummocky reflections (SF1) in their flanks,
344 unlike the layer-parallel, low-moderate amplitude reflections within the flanks of hydrothermal vents
345 (e.g. Fig. 10). Additionally, the eye-type hydrothermal vents described by Planke *et al.* (2005) have
346 inwardly dipping reflections in their lower parts, unlike the cone-shaped volcanoes in this study.
347 Moreover, the volcanoes we describe have zones of seismic velocity pull-up beneath them (Fig. 10),
348 a feature unreported for hydrothermal vents. It is also important to note that not all the volcanoes
349 we describe are linked to sills, and most are interpreted to have been fed by dykes (see section 5.1).
350 This spatial association is unlike that of hydrothermal vents, which are most commonly associated
351 with mafic sills (e.g. Svensen *et al.*, 2004; Planke *et al.* 2005; Hansen., 2006; Grove, 2013; Magee *et*
352 *al.*, 2013a; Schofield *et al.*, 2015; Alvarenga *et al.*, 2016).

353 Our mapping of the TV1, TV2 and TV3 horizons also indicates that multiple episodes of vent
354 formation occurred within the Bass Basin. This is typical of onshore volcanic activity in the Newer
355 Volcanics Province, where volcanism occurred from the Miocene through to the Holocene,
356 producing over 400 volcanoes (Boyce *et al.*, 2014) and no hydrothermal vents. In contrast,

357 hydrothermal vents along the northeast Atlantic margin are commonly found at a consistent
358 stratigraphic level (Svensen *et al.*, 2004). We therefore suggest that the timing of vent formation
359 within a basin can also help to distinguish between volcanoes and hydrothermal vents.

360 Whilst the lithology of the cone-shaped vents and the character of their seismic reflections
361 enable them to be distinguished from hydrothermal structures, determining the origin of crater-type
362 vents is more difficult. Seismic data is typically unable to image the dykes that underlie maars (cf.
363 Wall *et al.*, 2010) and both maars and hydrothermal vents produce excavations at the paleo-surface
364 due to blow-out of material. The association of maars with cone-shaped volcanoes, such as described
365 in this study, may help distinguish these features in other data sets.

366

367 **7. Summary**

368 The southern margin of Australia is typified by monogenetic, intraplate volcanism. We use 3D
369 seismic and well data from the Bass Basin, offshore northern Tasmania, to detail the architecture of
370 Miocene-aged submarine monogenetic volcanoes. The seismic characteristics of the volcanoes are
371 typical of volcanoclastic material, suggesting that they are composed of hyaloclastite and/or
372 pyroclasts, consistent with descriptions from well reports. The volcanoes evolved from crater-type
373 to cone-shaped vents perhaps as a consequence of variations in the efficiency of magma-water
374 interaction. We highlight that the morphology of the volcanoes are superficially similar to those
375 reported for hydrothermal vents documented from other volcanic-affected basins. We suggest the
376 internal seismic facies of vent structures, their lithology, relationship to the magma plumbing system
377 and the diachroneity of their emplacement can be used to determine the genesis of vents in other
378 datasets.

379

380 **Acknowledgements**

381 Clayton Grove and Joe Cartwright are thanked for constructive reviews and Cynthia Ebinger is
382 thanked for editorial handling. IHS Kingdom is thanked for software. Hess Company are thanked for
383 funding through the Volcanic Margins Research Consortium.

384

385 **Conflict of Interest**

386 No conflict of interest declared.

387

388 **8. References**

389 ALVARENGA, R., IACOPINI, D., KUCHLE, J., SCHERER, C. & GOLDBERG, K. (2016) Seismic Characteristics
390 and Distribution of Hydrothermal Vent Complexes in the Cretaceous Offshore Rift
391 Section of the Campos Basin, Offshore Brazil. *Marine and Petroleum Geology*.

392 BALL, P., EAGLES, G., EBINGER, C., MCCLAY, K. & TOTTERDELL, J. (2013) The Spatial and Temporal
393 Evolution of Strain During the Separation of Australia and Antarctica. *Geochemistry,*
394 *Geophysics, Geosystems*, **14**, 2771-2799.

395 BATIZA, R. & WHITE, J.D.L. (2000) Submarine Lavas and Hyaloclastite. In: *Encyclopedia of Volcanoes*
396 (Ed. by H. Sigurdsson). Academic Press.

397 BELL, B. & BUTCHER, H. (2002) On the Emplacement of Sill Complexes: Evidence from the Faroe-
398 Shetland Basin. *Geological Society, London, Special Publications*, **197**, 307-329.

399 BLEVIN, J. (2003) (Compiler) Petroleum Geology of the Bass Basin - Interpretation Report, an
400 Output of the Western Tasmanian Regional Minerals Program. . *Geoscience Australia, Record*
401 *2003/19*, ISSN: 1448-2177.

402 BOREEN, T.D. & JAMES, N.P. (1995) Stratigraphic Sedimentology of Tertiary Cool-Water
403 Limestones, Se Australia. *Journal of Sedimentary Research*, **65**.

404 BOYCE, J., KEAYS, R., NICHOLLS, I. & HAYMAN, P. (2014) Eruption Centres of the Hamilton Area of
405 the Newer Volcanics Province, Victoria, Australia: Pinpointing Volcanoes from a
406 Multifaceted Approach to Landform Mapping. *Australian Journal of Earth Sciences*, **61**, 735-
407 754.

408 CALVÈS, G., SCHWAB, A.M., HUUSE, M., CLIFT, P.D., GAINA, C., JOLLEY, D., TABREZ, A.R. & INAM, A.
409 (2011) Seismic Volcanostratigraphy of the Western Indian Rifted Margin: The Pre-Deccan
410 Igneous Province. *Journal of Geophysical Research: Solid Earth (1978–2012)*, **116**.

411 CAS, R., SATŌ, H. & SIMPSON, C.J. (1993) Newer Volcanics Province-Processes and Products of
412 Phreatomagmatic Activity: lavcei, Canberra 1993: Excursion Guide. *Australian Geological*
413 *Survey Organisation*.

414 CONNOR, C.B. & CONWAY, F.M. (2000) Basaltic Volcanic Fields. *Encyclopedia of volcanoes*, 331-343.
415 (Ed. by H. Sigurdsson). Academic Press.

416 DAVIES, R., BELL, B.R., CARTWRIGHT, J.A. & SHOULDERS, S. (2002) Three-Dimensional Seismic Imaging
417 of Paleogene Dike-Fed Submarine Volcanoes from the Northeast Atlantic Margin. *Geology*,
418 **30**, 223-226.

419 DAVIES, R.J., MACLEOD, C.J., MORGAN, R. & BRIGGS, S.E. (2005) Termination of a Fossil Continent-
420 Ocean Fracture Zone Imaged with Three-Dimensional Seismic Data: The Chain Fracture
421 Zone, Eastern Equatorial Atlantic. *Geology*, **33**, 641-644.

422 DAVIES, D., RAWLINSON, N., IAFFALDANO, G. & CAMPBELL, I. (2015) Lithospheric Controls on Magma
423 Composition Along Earth/'S Longest Continental Hotspot Track. *Nature*, **525**, 511-514.

424 EBINGER, C., DEINO, A., DRAKE, R. & TESH, A. (1989) Chronology of Volcanism and Rift Basin
425 Propagation- Rungwe Volcanic Province, East Africa. *Journal of Geophysical Research*, **94**,
426 15785-15803.

427 FOX, J., MC PHIE, J. & CAREY, R. (2016) Cape Grim, Nw Tasmania - a World Class Example of
428 Submarine Basaltic Intraplate Volcanism. Australian Earth Sciences Convention, Adelaide.

429 GROVE, C. (2013) Submarine Hydrothermal Vent Complexes in the Paleocene of the Faroe-
430 Shetland Basin: Insights from Three-Dimensional Seismic and Petrographical Data. *Geology*,
431 **41**, 71-74.

432 HANSEN, D.M. (2006) The Morphology of Intrusion-Related Vent Structures and Their Implications
433 for Constraining the Timing of Intrusive Events Along the Ne Atlantic Margin. *Journal of the*
434 *Geological Society*, **163**, 789-800.

435 HOLFORD, S., SCHOFIELD, N., MACDONALD J.D, DUDDY I.R & P.F, G. (2007) Seismic Analysis of
436 Igneous Systems in Sedimentary Basins and Their Impacts on Hydrocarbon Prospectivity:
437 Examples from the Southern Australian Margin.

438 HOLFORD, S., SCHOFIELD, N., MACDONALD, J., DUDDY, I. & GREEN, P. (2012) Seismic Analysis of
439 Igneous Systems in Sedimentary Basins and Their Impacts on Hydrocarbon Prospectivity:
440 Examples from the Southern Australian Margin. *Australian Petroleum Production and*
441 *Exploration Association Journal*, **52**, 229-252.

442 HOLT, S., HOLFORD, S. & FODEN, J. (2013) New Insights into the Magmatic Plumbing System of the
443 South Australian Quaternary Basalt Province from 3d Seismic and Geochemical Data.
444 *Australian Journal of Earth Sciences*, **60**, 797-817.

445 JACKSON, C.A.L. (2012) Seismic Reflection Imaging and Controls on the Preservation of Ancient
446 Sill-Fed Magmatic Vents. *Journal of the Geological Society*, **169**, 503-506.

447 JAMTVEIT, B., SVENSEN, H., PODLADCHIKOV, Y.Y. & PLANKE, S. (2004) Hydrothermal Vent Complexes
448 Associated with Sill Intrusions in Sedimentary Basins. *Physical geology of high-level magmatic*
449 *systems*, **234**, 233-241.

450 JERRAM, D.A. (2002) Volcanology and Facies Architecture of Flood Basalts. *Geological Society of*
451 *America Special Papers*, **362**, 119-132.

452 JOHNSON, R.W. (1989) *Intraplate Volcanism in Eastern Australia and New Zealand*. Cambridge
453 University Press.

454 KOKELAAR, P. (1986) Magma-Water Interactions in Subaqueous and Emergent Basaltic. *Bulletin of*
455 *Volcanology*, **48**, 275-289.

456 MAGEE, C., BRIGGS, F. & JACKSON, C.A. (2013a) Lithological Controls on Igneous Intrusion-Induced
457 Ground Deformation. *Journal of the Geological Society*, **170**, 853-856.

458 MAGEE, C., HUNT-STEWART, E. & JACKSON, C.A.-L. (2013b) Volcano Growth Mechanisms and the
459 Role of Sub-Volcanic Intrusions: Insights from 2d Seismic Reflection Data. *Earth and*
460 *Planetary Science Letters*, **373**, 41-53.

461 MAGEE, C., DUFFY, O.B., PURNELL, K., BELL, R.E., JACKSON, C.A.L. & REEVE, M.T. (2015) Fault-
462 Controlled Fluid Flow Inferred from Hydrothermal Vents Imaged in 3d Seismic Reflection
463 Data, Offshore Nw Australia. *Basin Research*, **20**.

464 MARESH, J., WHITE, R.S., HOBBS, R.W. & SMALLWOOD, J.R. (2006) Seismic Attenuation of Atlantic
465 Margin Basalts: Observations and Modeling. *Geophysics*, **71**, B211-B221.

466 MCCLINTOCK, M., WHITE, J.D.L., HOUGHTON, B.F. & SKILLING, I.P. (2008) Physical Volcanology of a
467 Large Crater-Complex Formed During the Initial Stages of Karoo Flood Basalt Volcanism,
468 Sterkspruit, Eastern Cape, South Africa. *Journal of Volcanology and Geothermal Research*, **172**,
469 93-111.

470 MEEUWS, F., HOLFORD, S., FODEN, J. & SCHOFIELD, N. (2016) Distribution, Chronology and Causes of
471 Cretaceous–Cenozoic Magmatism Along the Magma-Poor Rifted Southern Australian
472 Margin: Links between Mantle Melting and Basin Formation. *Marine and Petroleum Geology*,
473 **73**, 271-298.

- 474 MOORE, J.G. (1985) Structure and Eruptive Mechanisms at Surtsey Volcano, Iceland. *Geological*
475 *Magazine*, **122**, 649-661.
- 476 MUIRHEAD, J.D., EATON, A.R., RE, G., WHITE, J.D.L. & ORT, M.H. (2016) Monogenetic Volcanoes Fed
477 by Interconnected Dikes and Sills in the Hopi Buttes Volcanic Field, Navajo Nation, USA.
478 *Bulletin of Volcanology*, **78**, 1-16.
- 479 NELSON, C.E., JERRAM, D.A. & HOBBS, R.W. (2009) Flood Basalt Facies from Borehole Data:
480 Implications for Prospectivity and Volcanology in Volcanic Rifted Margins. *Petroleum*
481 *Geoscience*, **15**, 313-324.
- 482 PLANKE, S. & ELDHOLM, O. (1994) Seismic Response and Construction of Seaward Dipping Wedges
483 of Flood Basalts: Vøring Volcanic Margin. *Journal of Geophysical Research: Solid Earth (1978–*
484 *2012)*, **99**, 9263-9278.
- 485 PLANKE, S., SYMONDS, P.A., ALVESTAD, E. & SKOGSEID, J. (2000) Seismic Volcanostratigraphy of Large-
486 Volume Basaltic Extrusive Complexes on Rifted Margins. *Journal of Geophysical Research*,
487 **105**, 19335-19351.
- 488 PLANKE, S., RASMUSSEN, T., REY, S. & MYKLEBUST, R. (2005). Seismic Characteristics and Distribution
489 of Volcanic Intrusions and Hydrothermal Vent Complexes in the Vøring and Møre Basins.
490 *Geological Society, London, Petroleum Geology Conference series*, Geological Society of London.
491 **6**, 833-844.
- 492 RATEAU, R., SCHOFIELD, N. & SMITH, M. (2013) The Potential Role of Igneous Intrusions on
493 Hydrocarbon Migration, West of Shetland. *Petroleum Geoscience*, **19**, 259-272.
- 494 RE, G., WHITE, J. & ORT, M.H. (2015) Dikes, Sills, and Stress-Regime Evolution During Emplacement
495 of the Jagged Rocks Complex, Hopi Buttes Volcanic Field, Navajo Nation, USA. *Journal of*
496 *Volcanology and Geothermal Research*, **295**, 65-79.

- 497 SAAR, M.O. & MANGA, M. (1999) Permeability-Porosity Relationship in Vesicular Basalts. *Geophys.*
498 *Res. Lett.*, **26**, 111-114.
- 499 SCHOFIELD, N., HOLFORD, S., MILLETT, J., BROWN, D., JOLLEY, D., R. PASSEY, S., MUIRHEAD, D., GROVE,
500 C., MAGEE, C., MURRAY, J., HOLE, M., A.-L. JACKSON, C. & STEVENSON, C. (2015) Regional
501 Magma Plumbing and Emplacement Mechanisms of the Faroe-Shetland Sill Complex:
502 Implications for Magma Transport and Petroleum Systems within Sedimentary Basins. *Basin*
503 *Research*, n/a-n/a.
- 504 SCHUTTER, S.R. (2003) Hydrocarbon Occurrence and Exploration in and around Igneous Rocks.
505 *Geological Society, London, Special Publications*, **214**, 7-33.
- 506 SIGURDSSON, H., HOUGHTON, B., MCNUTT, S., RYMER, H. & STIX, J. (2015) *The Encyclopedia of*
507 *Volcanoes*. Elsevier.
- 508 SUITING, I. & SCHMINCKE, H.-U. (2009) Internal Vs. External Forcing in Shallow Marine Diatreme
509 Formation: A Case Study from the Iblean Mountains (Se-Sicily, Central Mediterranean).
510 *Journal of Volcanology and Geothermal Research*, **186**, 361-378.
- 511 SUITING, I. & SCHMINCKE, H.U. (2012) Iblean Diatremes 3: Volcanic Processes on a Miocene
512 Carbonate Platform (Iblean Mountains, Se-Sicily): A Comparison of Deep Vs. Shallow Marine
513 Eruptive Processes. *Bulletin of Volcanology*, **74**, 207-230.
- 514 SUTHERLAND, F. & WELLMAN, P. (1986). Potassium-Argon Ages of Tertiary Volcanic Rocks,
515 Tasmania. *Papers and Proceedings of the Royal Society of Tasmania*, **120**, 77-86.
- 516 SVENSEN, H., PLANKE, S., JAMTVEIT, B. & PEDERSEN, T. (2003) Seep Carbonate Formation Controlled
517 by Hydrothermal Vent Complexes: A Case Study from the Vøring Basin, the Norwegian
518 Sea. *Geo-Marine Letters*, **23**, 351-358.

- 519 SVENSEN, H., PLANKE, S., MALTHER-SØRENSEN, A., JAMTVEIT, B., MYKLEBUST, R., RASMUSSEN EIDEM, T. &
520 REY, S.S. (2004) Release of Methane from a Volcanic Basin as a Mechanism for Initial Eocene
521 Global Warming. *Nature*, **429**, 542-545.
- 522 SVENSEN, H., JAMTVEIT, B., PLANKE, S. & CHEVALLIER, L. (2006) Structure and Evolution of
523 Hydrothermal Vent Complexes in the Karoo Basin, South Africa. *Journal of the Geological*
524 *Society*, **163**, 671-682.
- 525 SVENSEN, H., PLANKE, S., CHEVALLIER, L., MALTHER-SØRENSEN, A., CORFU, F. & JAMTVEIT, B. (2007)
526 Hydrothermal Venting of Greenhouse Gases Triggering Early Jurassic Global Warming.
527 *Earth and Planetary Science Letters*, **256**, 554-566.
- 528 THOMSON, K. & HUTTON, D. (2004) Geometry and Growth of Sill Complexes: Insights Using 3d
529 Seismic from the North Rockall Trough. *Bulletin of Volcanology*, **66**, 364-375.
- 530 THOMSON, K. (2007) Determining Magma Flow in Sills, Dykes and Laccoliths and Their Implications
531 for Sill Emplacement Mechanisms. *Bulletin of Volcanology*, **70**, 183-201.
- 532 THORDARSON, T. & SELF, S. (1993) The Laki (Skaftár Fires) and Grímsvötn Eruptions in 1783–1785.
533 *Bulletin of Volcanology*, **55**, 233-263.
- 534 TOTTERDELL, J. & BRADSHAW, B. (2004). *The Structural Framework and Tectonic Evolution of the Bight*
535 *Basin*. Eastern Australasian Basins Symposium II. Petroleum Exploration Society of Australia,
536 Special Publication, 41-61.
- 537 TRIGG, K.R., BLEVIN, J.E. & BOREHAM, C. (2003) An Audit of Petroleum Wells in the Bass Basin
538 1965-1999, Geoscience Australia Record 2003/11 ISSN: 1039-0073.
- 539 VALENTINE, G.A. & CORTÉS, J.A. (2013) Time and Space Variations in Magmatic and
540 Phreatomagmatic Eruptive Processes at Easy Chair (Lunar Crater Volcanic Field, Nevada,
541 USA). *Bulletin of volcanology*, **75**, 1-13.

- 542 WALL, M., CARTWRIGHT, J., DAVIES, R. & MCGRANDLE, A. (2010) 3d Seismic Imaging of a Tertiary
543 Dyke Swarm in the Southern North Sea, Uk. *Basin Research*, **22**, 181-194.
- 544 WATTON, T.J., JERRAM, D.A., THORDARSON, T. & DAVIES, R.J. (2013a) Three-Dimensional Lithofacies
545 Variations in Hyaloclastite Deposits. *Journal of Volcanology and Geothermal Research*, **250**,
546 19-33.
- 547 WATTON, T.J., WRIGHT, K.A., JERRAM, D.A. & BROWN, R.J. (2013b) The Petrophysical and
548 Petrographical Properties of Hyaloclastite Deposits: Implications for Petroleum
549 Exploration. *AAPG Bulletin*, **98**, 449-463.
- 550 WHITE, J.D. & ROSS, P.-S. (2011) Maar-Diatreme Volcanoes: A Review. *Journal of Volcanology and*
551 *Geothermal Research*, **201**, 1-29.
- 552 WRIGHT, K.A., DAVIES, R.J., JERRAM, D.A., MORRIS, J. & FLETCHER, R. (2012) Application of Seismic and
553 Sequence Stratigraphic Concepts to a Lava-Fed Delta System in the Faroe-Shetland Basin,
554 Uk and Faroes. *Basin Research*, **24**, 91-106.
- 555 ZHAO, F., WU, S., SUN, Q., HUUSE, M., LI, W. & WANG, Z. (2014) Submarine Volcanic Mounds in the
556 Pearl River Mouth Basin, Northern South China Sea. *Marine Geology*, **355**, 162-172.

557

558 **Fig. 1.** (a) Location map of the Labatt and Yolla surveys in the Basin Basin. Bathymetric contours
559 are in metres. (b) Map showing the distribution of Eocene-Recent-aged basalts, onshore southern
560 Australia. Modified from Johnson, R. W., 1989. (c) Stratigraphic column, also showing seismic
561 horizons picked in this study.

562 **Fig. 2.** 2D seismic line (a) and interpretation (b) connecting the Labatt and Yolla surveys.

563 **Fig. 3.** Seismic section showing the correlation between seismic data and the Yolla-I and Bass-I
564 wells. Adapted from Trigg, K. R. *et al.* (2003).

565 **Fig. 4.** Time map of the TV2 and TV1 surfaces in the Labatt (a) and Yolla (b) surveys.

566 **Fig. 5.** Seismic line and interpretation through the Labatt survey. See Fig. 4 for location. TV2=Top
567 Volcanic, BV2=Base Volcanic, EVCM= Eastern View Coal Measures.

568 **Fig. 6.** Seismic line and interpretation through the Yolla survey. See Fig. 4 for location. TV1=Top
569 Volcanic, BVI=Base Volcanic, EVCM= Eastern View Coal Measures.

570 **Fig. 7.** Seismic sections and interpretive sketches of crater-type (a), pointed (b), flat-topped (c) and
571 cratered (d) vents. See Fig. 4 for their location. Graphs (e) and (f) show the relationship between
572 vent volume and height and basal diameter for the cone-type vents.

573 **Fig. 8.** Seismic cross section of a vent fed by a sill. TV2=Top Volcanic, BV2=Base Volcanic. See Fig.
574 4 for location.

575 **Fig. 9.** Schematic diagram showing the evolution of the volcanoes from pit craters (maars) (a), to
576 pointed-types (pillow volcanoes) (b) and finally cratered and flat-topped types (tuff cones) (c).

577 **Fig. 10.** Seismic cross section of a hydrothermal vent (a) located on the Northeast Atlantic margin.
578 An increase in acoustic impedance is represented by a blue reflection. Modified from Schofield, N.
579 *et al.*, 2015. (b) Seismic cross section from a volcano in this study. A red reflection represents an
580 increase in acoustic impedance. See Fig. 4 for location.

581 **Table 1.** Compilation of well data showing the volcanic intervals found in Bass Basin exploration
582 wells. Compiled from Blevin, J. (2003) and Trigg, K. R. *et al.*, (2003).

583 **Table 2.** Summary of the morphology of the vents observed in this study.

584 **Table 3.** Characteristics of vent structures observed in seismic data. ⁽¹⁾ Compiled from Planke, S. *et*
585 *al.* 2005; Hansen, D. M., 2006; Svensen, H. *et al.*, 2006 and Grove, C., 2013. ⁽²⁾ From Magee, C. *et al.*,
586 2013b. ⁽³⁾ From Wall, M. *et al.* 2010. ⁽⁴⁾ From Bell, B. & Butcher, H., 2002. *calculated using depths in
587 time from Planke, S. *et al.* 2005 and a velocity of 3 km s⁻¹

588

Well	Depth below KB volcanic material intersected (m)	Water depth (m)	KB elevation (m)	Description	Inferred age
Aroo-1	3150–3600	76	9.8	Weathered basaltic flows interbedded with sandstones	Late Cretaceous to Palaeocene
Bass-1	790–950	81	No data	Pyroclastic material	Miocene
Bass-2	1679–1757	85	No data	Intrusion	Unknown
Chat-1	>3000	81	25	Volcanics	Late Cretaceous to Palaeocene
Cormorant-1	2450–2600	73	30	Volcanics and olivine gabbro sill	Miocene
Durroon-1	1584–1591; 1542–1645	68	10	Volcaniclastic sandstone	Early Cretaceous
Flinders-1	2200–2290	69	No data	Dolerite intrusion	Miocene
Koorkha-1	2100–2140	67	22	Basaltic intrusion	Eocene
Seal-1	1500–1600; >1650	64	25	Dolerite intrusion	Miocene
Silvereye-1	As metre-thick intervals between 1290–1425 and 2110–2300	54	No data	Altered, blocky volcanics, possibly of pyroclastic origin, also dolerite	Eocene
Squid-1	2350–2390	80	22	Alkali olivine basalt intrusion	Unknown
Tasmanian Devil-1	>750	74	22	Basalts	Palaeocene
Tilana-1	1250–1400 2000–2250 >3100	79	22	Vesicular basalt; gabbro; basalt	Mid Eocene to Mid Oligocene; Early to Mid Eocene; Late Maastrichtian to Late Palaeocene
Toolka-1	2400–2700	78	9	Intrusion	Unknown
Yolla-1	1237–1305; >3000	79	11	Highly altered pyroclastics; doleritic intrusion	Miocene ; Late Cretaceous to Palaeocene

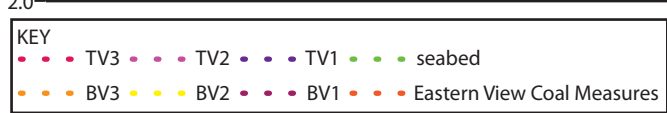
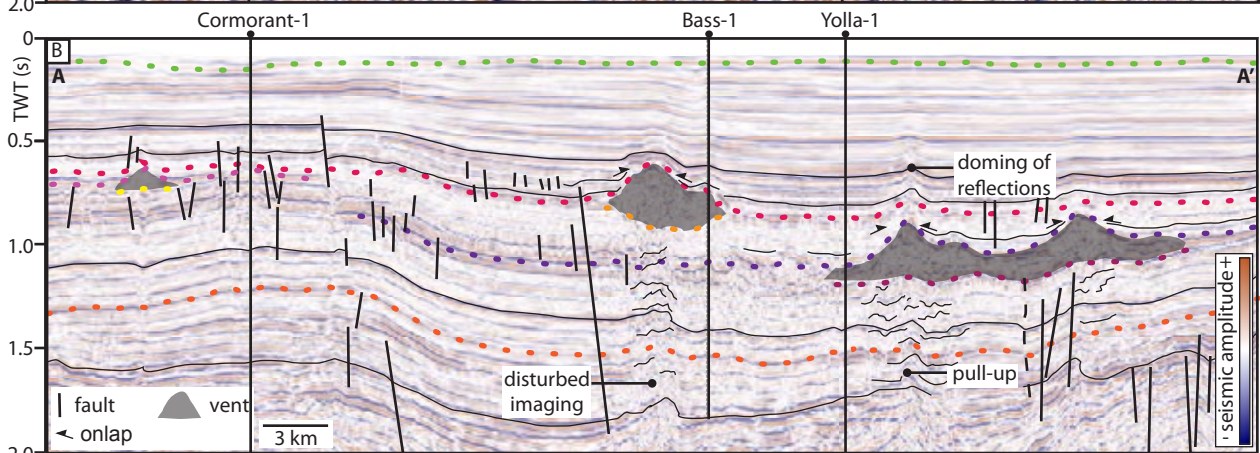
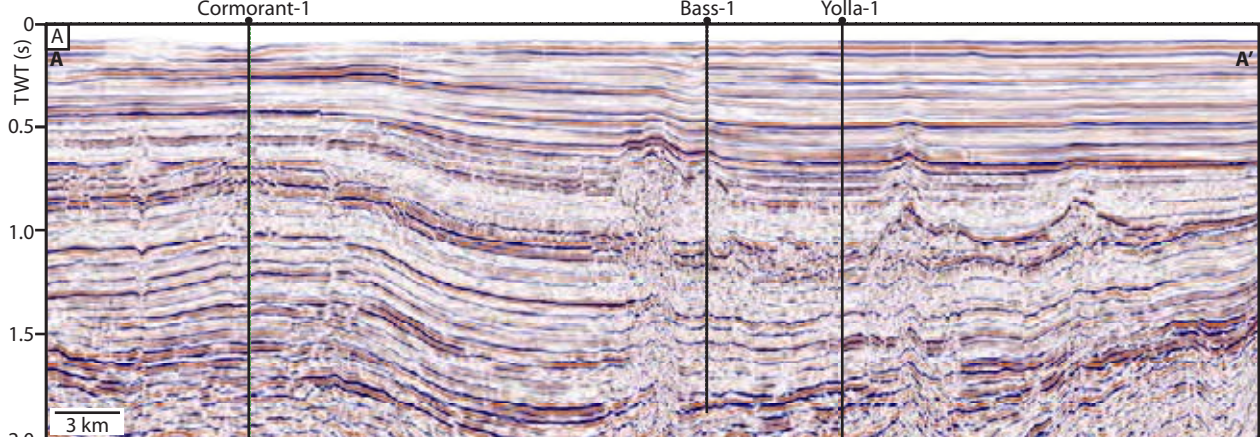
Table 1

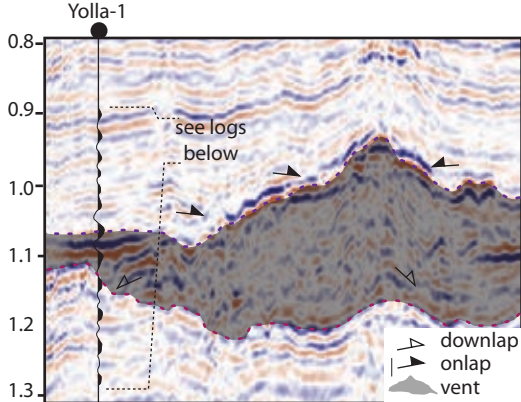
Vent morphology		n	Crater diameter (km)	Diameter (km)	Height (km)	Volume (km ³)
Crater-type	Crater	15	n/a	0.3–1.2	n/a	n/a
Cone type	Pointed	7	n/a	1–3	0.13–0.16	0.4–1.1
	Cratered	5	380–950	3–5	0.2–0.31	0.07–1.36
	Flat-topped	7	n/a	1–4	0.12–0.52	1–1.4

Table 2.

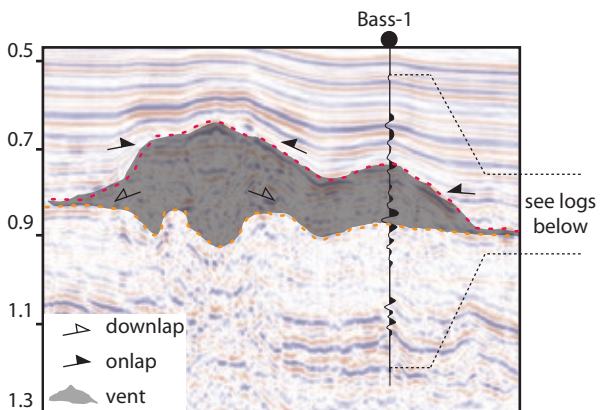
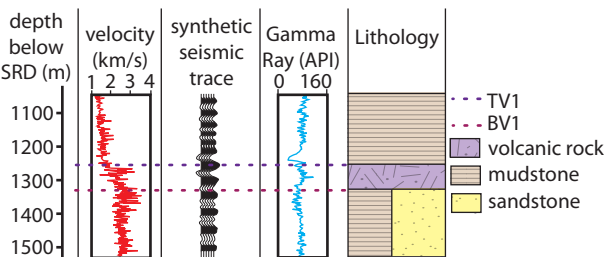
Vent type	Basal D (km)	Height (km)	Depth to underlying sill (km)	Dyke fed?	Morphology	Dominant lithology	Spatial Distribution	Basal relationship	Timing of emplacement	Internal reflections
Hydrothermal ⁽¹⁾	0.4–1	0.03–0.45	300–650 0*	No	Crater, eye or dome shaped	Diatomitic siltstone, carbonate and sandstone	Linear rows or isolated	Flat-lying concordant, downwarped concordant, truncated	Dominantly synchronous, pre-dating main stage of effusive activity	Chaotic, and low-moderate amplitude, sub-parallel reflections which downlap the pre-eruptive surface
Shield volcano ⁽²⁾	1.94–18.89	0.02–1	0.05–1.5	Yes	Cone-shaped with rounded or flat tops	Hyaloclastite, lava flows, interbedded sediments and minor intrusions	Linear rows or isolated	Upwarped concordant, flat-lying concordant	Not described	Chaotic, and low-high amplitude, sub-parallel reflections which downlap the pre-eruptive surface
Maar ⁽³⁾	0.2–1	Not described	N/A	Yes	Crater shaped	N/A	Linear rows	Truncated	Synchronous	Low-moderate amplitude, sub-parallel reflections which onlap crater wall
Seamount ⁽⁴⁾	≤2	>0.1	Not described	Not described	Cone-shaped	Pillow lava and hyaloclastite	Above sills	Flat-lying concordant	Not described	Low-high amplitude reflections which downlap the pre-eruptive surface
Tuff cones, pillow volcanoes and maars (this study)	0.3–5	0.12–0.52	495–1200	Yes	Cone-shaped with cratered, flat topped or pointed morphologies, also crater-shaped	Pyroclasts and hyaloclastite	Linear rows or isolated	Upwarped concordant, truncated	Diachronous	Chaotic, and moderate-high amplitude, hummocky reflections which downlap the pre-eruptive surface

Table 3.

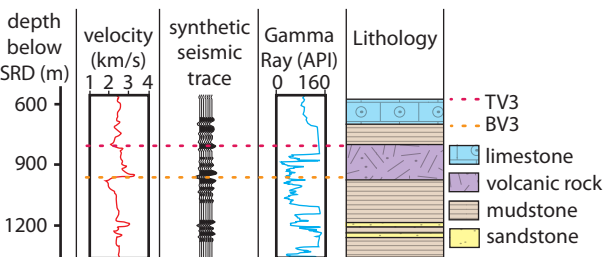


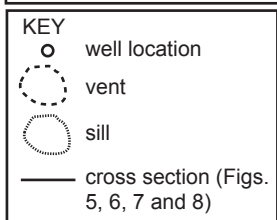
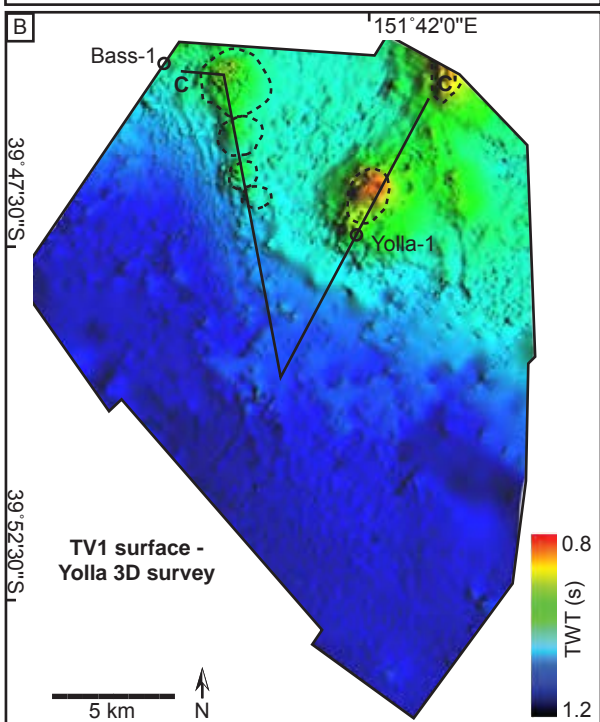
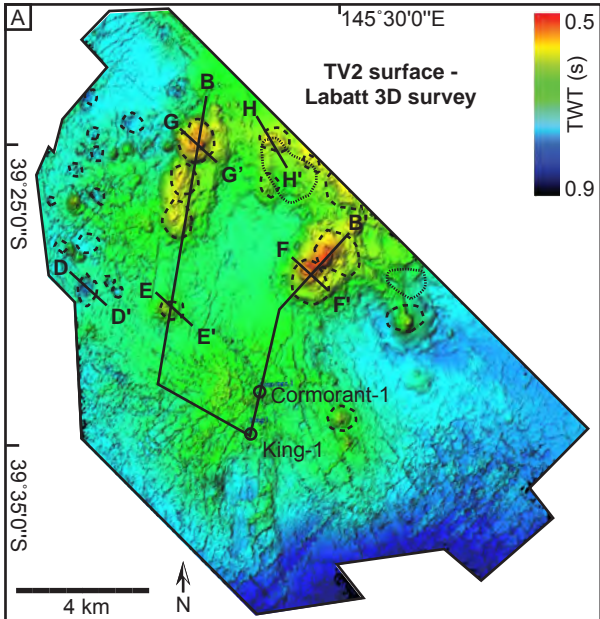


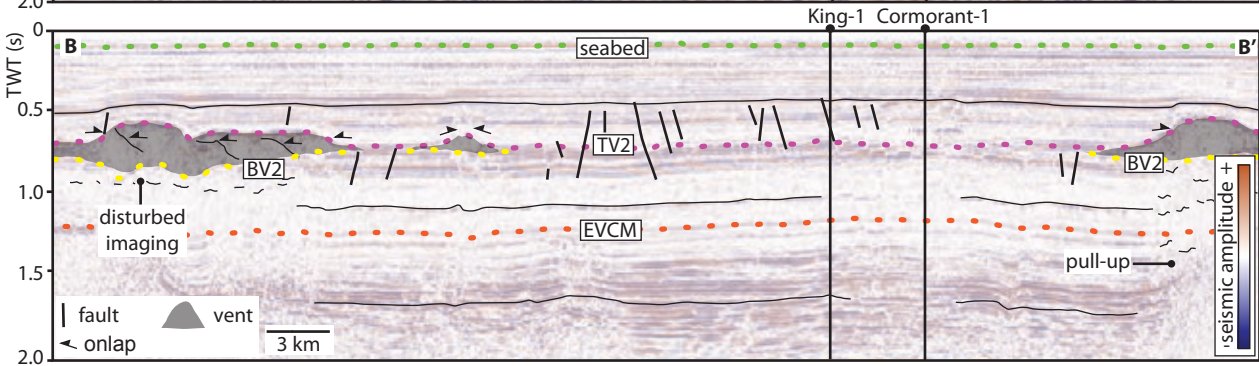
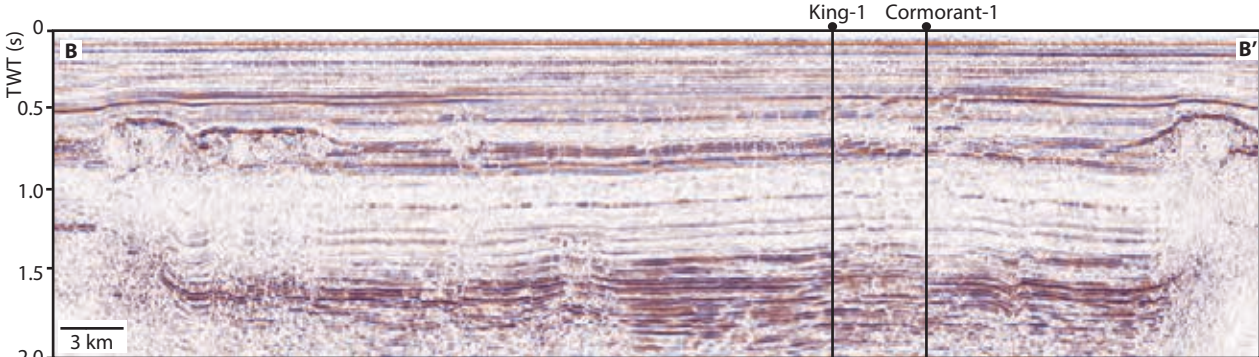
TWT (s)

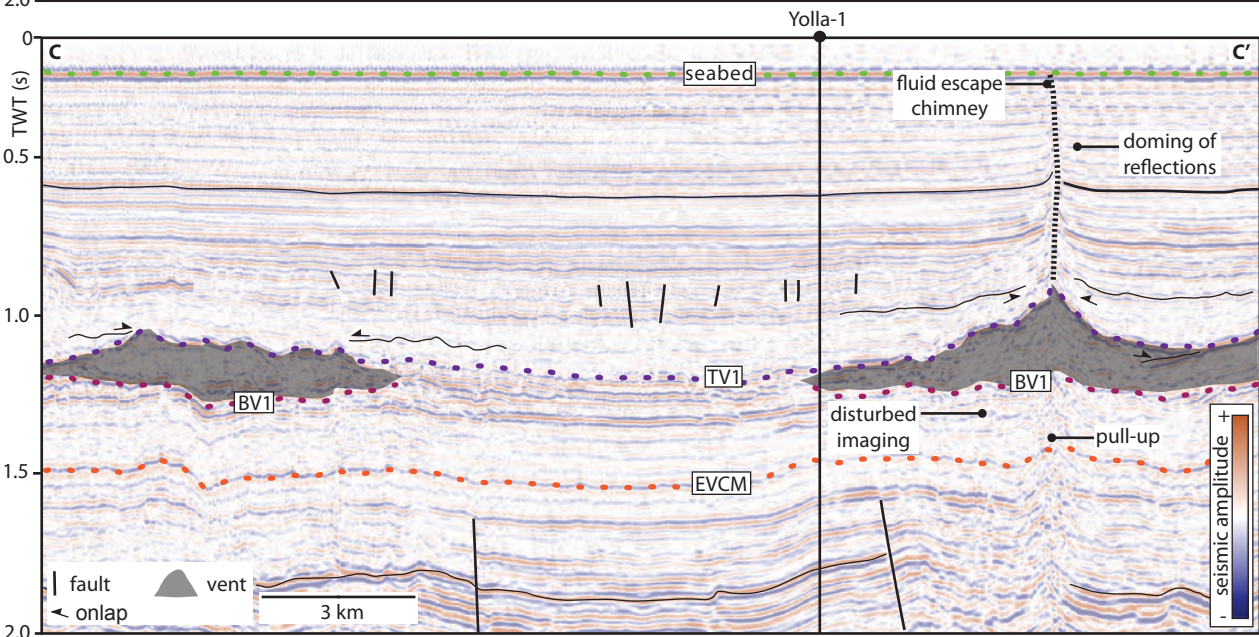
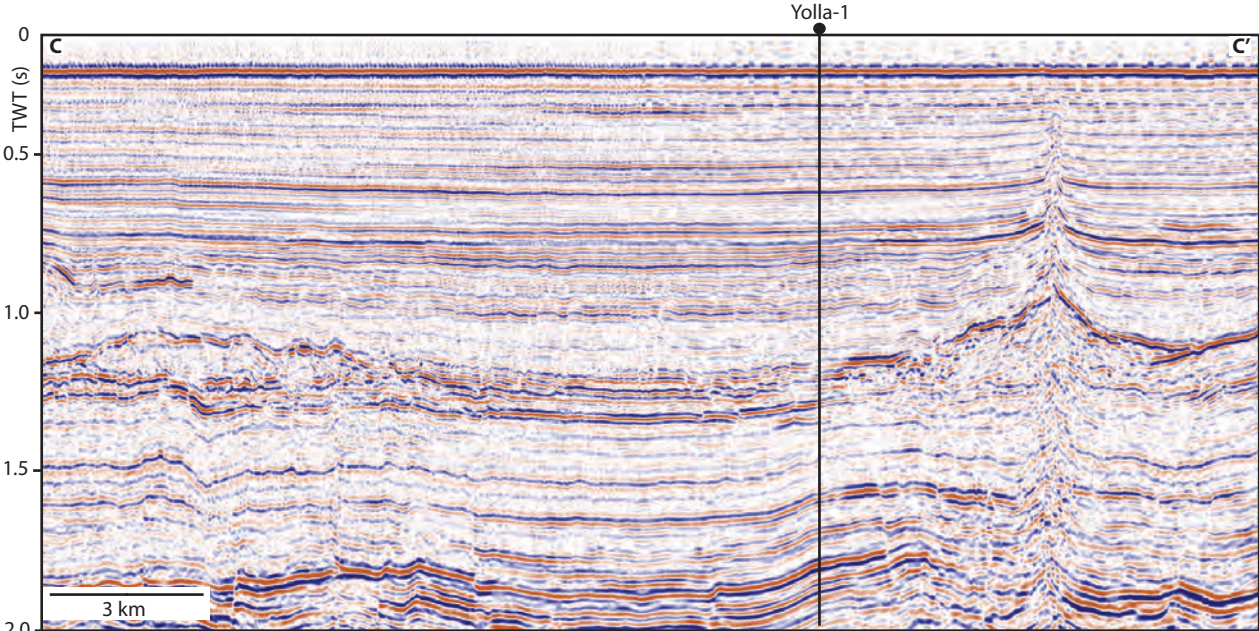


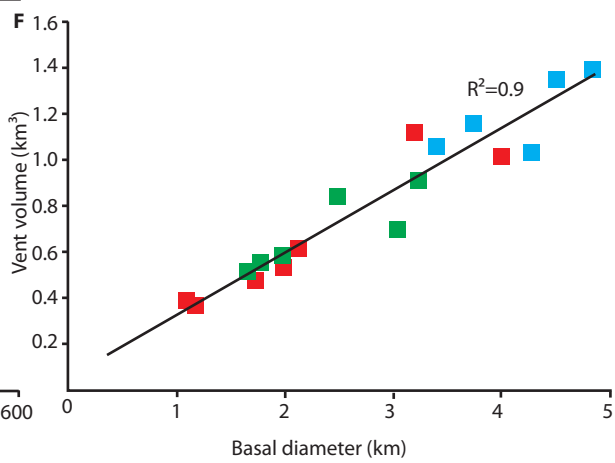
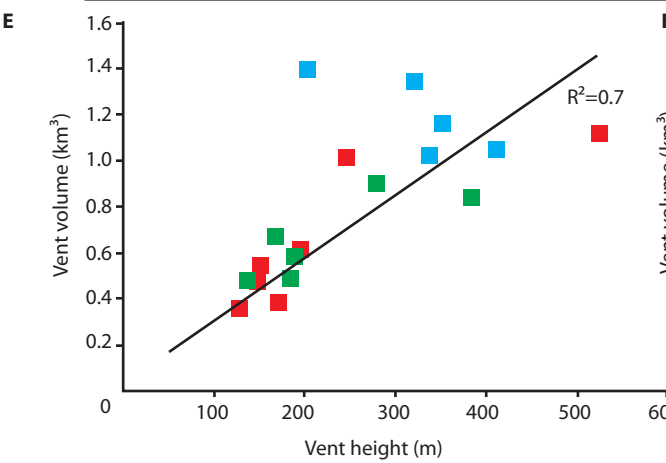
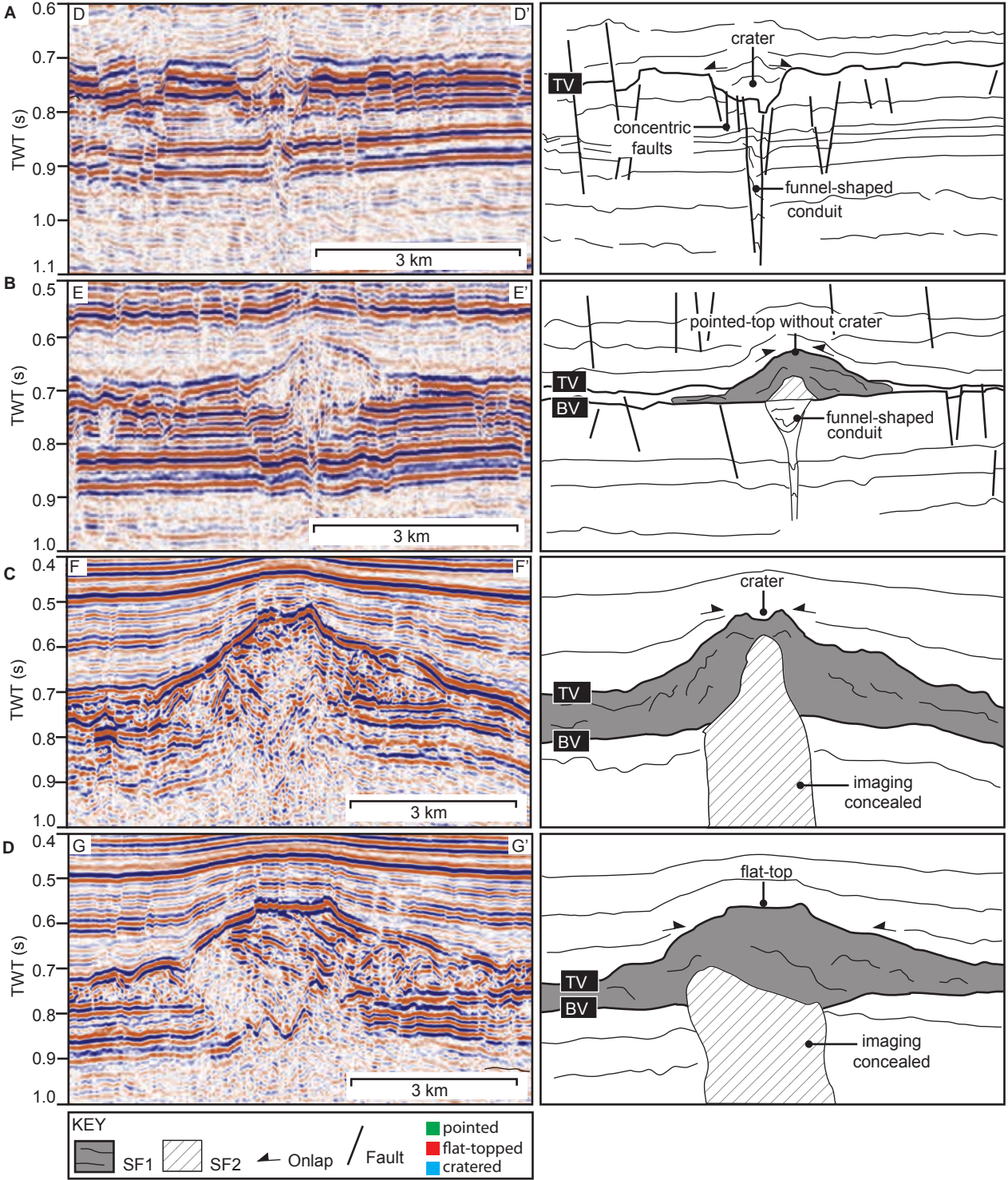
TWT (s)

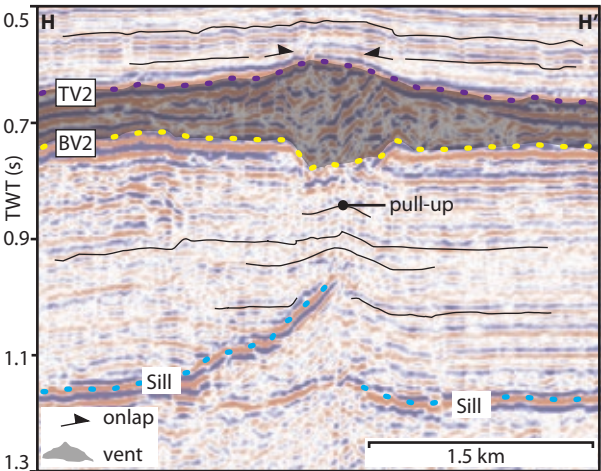




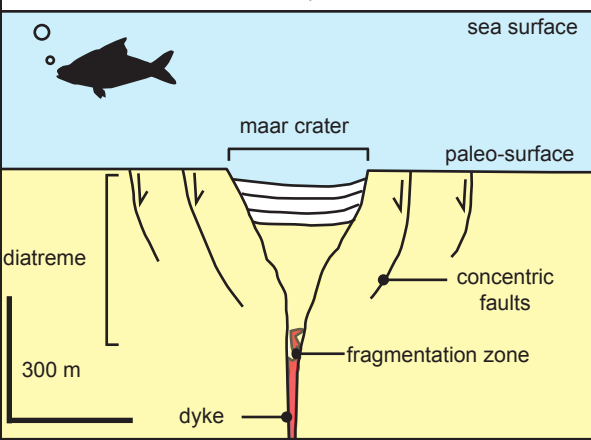




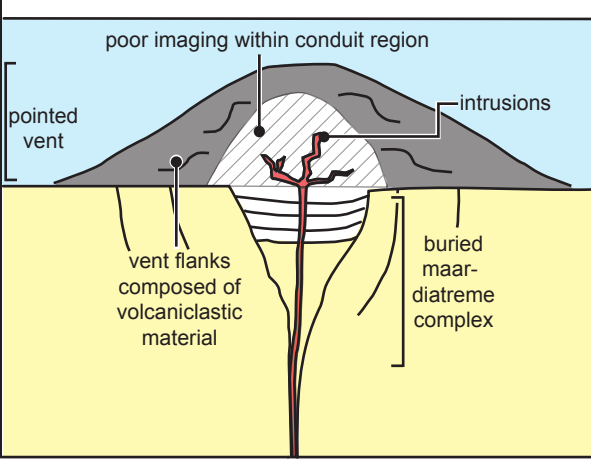




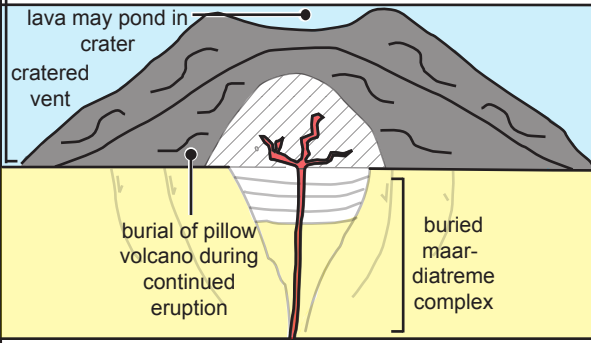
A Sub-surface magma fragmentation forms maar-diatreme complex



B Formation of pillow volcano during effusive activity



C Formation of tuff cone and decreasing hydrostatic pressure



SEISMIC FACIES

